PCCP

ROYAL SOCIETY OF CHEMISTRY

PAPER

Cite this: *Phys. Chem. Chem. Phys.*, 2026, **28**, 5948

Mode-specific quasi-classical dynamics of the F^- + SiH_3Cl system

Attila Á. Dékány, Balázs J. Molnár and Gábor Czakó *

Received 14th November 2025,
Accepted 7th February 2026

DOI: 10.1039/d5cp04412j

rsc.li/pccp

We conducted mode-specific quasi-classical trajectory (QCT) simulations of the gas-phase F^- + SiH_3Cl reaction employing a full-dimensional, coupled-cluster-quality potential energy surface. Simulations were performed at collision energies ranging from 1 to 40 kcal mol^{-1}, with one vibrational quantum selectively excited in each of the six distinct vibrational modes of SiH_3Cl, namely the SiCl stretching, SiH_3 rocking, SiH_3 umbrella and deformation modes, and symmetric and asymmetric SiH stretching. Multiple reaction channels were analyzed, including chloride-ion substitution *via* inversion and retention pathways, proton abstraction, hydrogen chloride (HCl) formation, hydride-ion substitution, molecular-hydrogen production, and $FHCl^-$ formation. From the QCT simulations, reaction probabilities, integral cross sections, initial attack angle and scattering angle distributions, and product energy distributions (internal, translational, vibrational, and rotational) were derived. Notably, excitation of SiH stretching modes led to a modest reduction in cross sections for chloride-ion substitution, whereas other product channels showed mild to significant enhancements. Excitation of other vibrational modes minimally impacted chloride-substitution and proton-abstraction cross sections, but significantly, although less markedly than SiH stretching modes, enhanced the remaining product channels. The initial attack angle and scattering angle distributions are not affected by vibrational excitations for all product channels, and the post-reaction energy distributions showed minimal effects.

Introduction

Studying vibrational mode-specificity and bond selectivity in chemical reactions has a long history starting with the simple H + HOD reaction[1] in the 1980s and arriving to more complex systems like the reactions of CH_4,[2–6] C_2H_6,[7–9] and CH_3OH[10] with atoms in the 1990s–2020s. Most of the mode-specific studies have been focused on neutral systems,[1–10] nevertheless, ion–molecule reactions[11–22] have also been investigated recently. Following several reduced-dimensional mode-specific quantum dynamics[11–13] and full-dimensional quasi-classical trajectory (QCT)[12] studies on the X^- + CH_3Y systems, where X and Y are halogens, in 2018 the Wester group carried out crossed-beam experiments for the F^- + CH_3I reaction revealing the effects of CH stretching excitation on the bimolecular nucleophilic substitution (S_N2) and proton-abstraction channels.[14] Since 2018 several additional experimental[16,17] and theoretical[15,18–22] mode-specific investigations have been performed for S_N2 reactions even going beyond the reactions of simple ions with methyl halides, see, for example, studies on OH^- + CH_3F/CH_3I[19–21] and F^- + CH_3CH_2Cl.[18] However, while all of these ion–molecule reactions proceed at carbon centers, mode-specific effects are basically unknown at other central atoms.

In 2023 we reported the first analytical *ab initio* potential energy surface (PES) for a silicon-centered ion–molecule reaction, namely for the F^- + SiH_3Cl system.[23] QCT simulations on this PES revealed complex dynamics involving HCl, H^-, $FHCl^-$, H_2, H_2 + Cl^-, and HF + Cl^- formation besides the major S_N2 and proton-abstraction channels leading to Cl^- and HF products, respectively.[23] Most of these channels are exothermic and proceed through submerged stationary points, therefore, it is unclear how initial vibrational excitations affect their reactivity and mechanisms. In many chemical reactions the position and energy of the transition state control the mode-specific dynamics, however, in the present case the S_N2 Walden-inversion pathway does not involve a transition state, but proceeds *via* a minimum complex.[23] Therefore, it is interesting to find out whether this complex plays a similar role as a transition state in carbon-centered S_N2 reactions. Furthermore, it is important to note that the above-mentioned alternative reaction channels usually have low cross sections.[23] Nevertheless, their reactivity may be significantly enhanced upon the excitation of specific vibrational modes of the reactant.

Following our detailed dynamics investigations on the ground-state F^- + SiH_3Cl reaction,[23,24] in the present work we

MTA-SZTE Lendület "Momentum" Computational Reaction Dynamics Research Group, Interdisciplinary Excellence Centre and Department of Physical Chemistry and Materials Science, Institute of Chemistry, University of Szeged, Rerrich Béla tér 1, Szeged H-6720, Hungary. E-mail: gczako@chem.u-szeged.hu

report a comprehensive vibrational mode-specific QCT study on the F^- + SiH_3Cl system utilizing our analytical PES.[23] By selectively exciting the various vibrational modes of the SiH_3Cl molecule at different collision energies, our simulations reveal the effects of initial translational and mode-specific vibrational energy on the reactivity, product branching, energy transfer, and mechanisms of the title reaction. In the next section we provide the computational details including the description of the initial normal modes. Then the key characteristics of the PES as well as the QCT results and their discussion are given. The paper ends with summary and conclusions.

Methods and computational details

We performed gas-phase quasi-classical trajectory (QCT) simulations of the F^- + SiH_3Cl system on a full-dimensional, coupled-cluster-quality potential energy surface (PES)[23] to investigate mode-specific vibrational excitation effects. The PES was developed and reported by our research group,[23] and it was obtained by fitting a permutationally invariant polynomial[25] to (CCSD-F12b + BCCD(T)–BCCD)/aug-cc-pVTZ quality energy points. The development process was partially automated out by the Robosurfer program package.[26] The *ab initio* calculations were performed by the 2015.1 version of the Molpro quantum chemistry software,[27] and the polynomial fitting was carried out by a Fortran library developed by Braams and Bowman.[25] The vibrational modes of the polyatomic reactant molecule, SiH_3Cl, were initialized *via* normal-mode sampling[28] while ensuring zero rotational energy at the initial step of the simulations. The vibrational energies were set so that in the excitation simulations, one selected mode was excited by one vibrational quantum. As a reference, vibrational ground state simulations were also run. This initial sampling can reveal the excitation effect of each mode on the dynamics. Studying the effects of the simultaneous excitation of two or more modes or vibrational overtones is out of the scope of the present work.

Collision energies were set to 1, 5, and subsequently up to 40 kcal mol^{-1} by 5 kcal mol^{-1} increments. Note that this translational energy interval is typical in similar ion–molecule reaction dynamics studies. For each fixed collision energy, impact parameters were sampled between 0 and b_{max} in 0.5 bohr increments, where b_{max} denotes the maximum impact parameter at a given collision energy beyond which only non-reactive trajectories are observed. The initial center-of-mass separation was defined as $\sqrt{x^2 + b^2}$, with x chosen as 40 bohr for collision energies of 1 and 5 kcal mol^{-1} and 25 bohr at higher collision energies, ensuring that the initial separation exceeded b_{max} in all cases.

For each combination of fixed collision energy and impact parameter, 5000 trajectories were propagated using the velocity Verlet algorithm[29] with a 3 $\hbar/E_h$ ($\approx$0.0726 fs) time step, where $\hbar$ is the reduced Planck constant and E_h is the hartree energy unit. All trajectory propagations were carried out using an in-house Fortran code developed for QCT simulations. The initial parameters of the trajectories were randomized with respect to the relative orientation of the reactants and the phases of their vibrational modes. The trajectories were post-processed using our Python analyzis package.[30,31]

Propagations were terminated when the maximum interatomic distance exceeded the initial maximum interatomic distance by 1 bohr, ensuring that the product fragments were noninteracting. Product identification was performed using atomic connectivity analyzis at the termination point. While this criterion is sufficient for two-fragment products, three-fragment configurations may remain ambiguous, as two fragments can still be in close proximity. In addition, transient bond elongations and vibrational distortions can lead to unidentifiable connectivity (*i.e.*, not corresponding to any reference structure). To resolve such cases, trajectories yielding three-fragment products or unidentified final geometries were propagated further for an additional fixed 20 thousand time steps. The final product assignment was taken from the earliest trajectory step exhibiting a well-defined fragmentation pattern, namely (i) an identifiable two-fragment configuration replacing a previously identified three-fragment or an unidentified configuration, or (ii) an identifiable three-fragment configuration replacing an unidentified one. If an unidentified configuration evolved sequentially into recognizable three- and then two-fragment products, the first two-fragment configuration was selected.

The definitions of the initial attack angle, scattering angle, and the product energy distribution analyzis follow our previous ground-state QCT study.[24] The initial attack angle (α) was defined at the beginning of each trajectory as the angle between the center-of-mass velocity vector of the SiH_3Cl reactant and the Si–Cl bond vector ($\mathbf{x}_{Cl} - \mathbf{x}_{Si}$, where $\mathbf{x}$ denotes an atomic position). By our definition $\cos(\alpha) = -1$ ($\alpha = 180^\circ$) corresponds to a backside approach toward the silicon center, and $\cos(\alpha) = 1$ ($\alpha = 0^\circ$) corresponds to a front-side approach, where the chlorine ligand facing toward the incoming F^- ion. The scattering angle (θ) is the angle between the initial center-of-mass velocity vector of the incoming fluoride ion and the final center-of-mass velocity vector of the fluorine-containing product. In two-fragment product channels, the conservation of momentum and the collinear center-of-mass velocity vectors of the reactants ensure that the velocity vectors of the product pair are collinear, therefore the scattering angle defined for one product uniquely determines that of the other. Distributions of both angles were obtained by binning the cosine of the corresponding angle into uniformly spaced intervals between -1 and 1.

A detailed description of the harmonic normal vibration modes of the reactant molecule is shown in Fig. 1. Wavenumbers are obtained at the PES[23] (ν_{PES}) and by direct *ab initio* ($\nu_{ab\ initio}$) calculations at the CCSD(T)-F12b/aug-cc-pVTZ level of theory,[32,33] respectively. A molecule with five atoms, such as SiH_3Cl, possesses nine linearly independent vibrational degrees of freedom. Due to the C_{3v} symmetry of SiH_3Cl, three of these modes are doubly degenerate, resulting in six energetically different vibrational modes. The lowest-energy vibrational mode is the SiCl stretch, with a wavenumber of ν_{PES} = 547 cm^{-1} ($\nu_{ab\ initio}$ = 552 cm^{-1}). This is followed by the doubly-degenerate SiH_3 rocking mode, with ν_{PES} = 690 cm^{-1} ($\nu_{ab\ initio}$ = 667 cm^{-1}). The SiH_3 umbrella and deformation

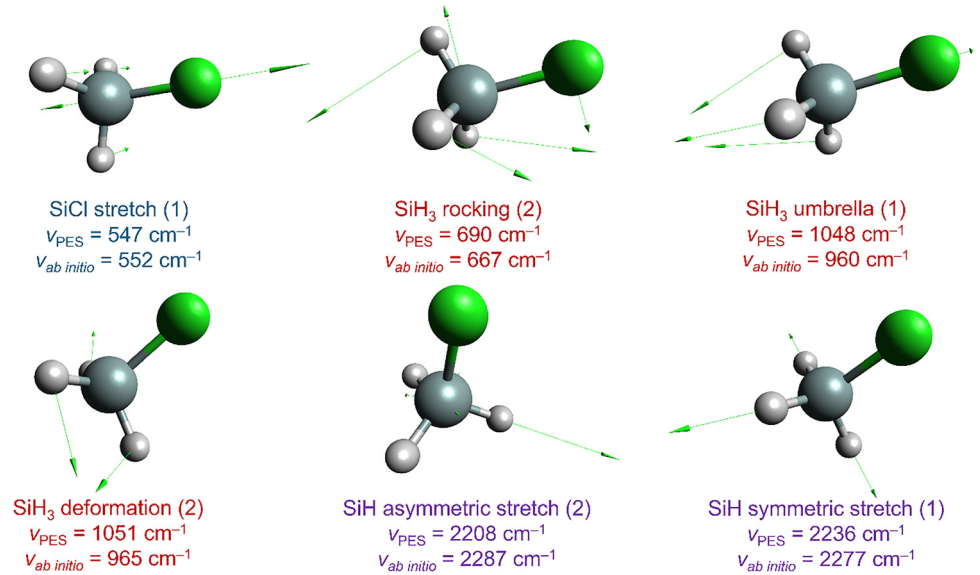

Fig. 1 Harmonic normal modes of vibration and their degeneracies in parentheses for the SiH_3Cl molecule obtained at a coupled-cluster-quality analytical potential energy surface[23] (ν_{PES}), and by direct *ab initio* computations at the CCSD(T)-F12b/aug-cc-pVTZ level of theory ($\nu_{ab\ initio}$).

modes have nearly identical energies, with ν_{PES} = 1048 cm^{-1} ($\nu_{ab\ initio}$ = 960 cm^{-1}) and 1051 cm^{-1} ($\nu_{ab\ initio}$ = 965 cm^{-1}), respectively. Of these two modes, the umbrella mode is non-degenerate. Finally, the asymmetric and symmetric SiH stretching modes exhibit the highest harmonic wavenumbers, at ν_{PES} = 2208 cm^{-1} ($\nu_{ab\ initio}$ = 2287 cm^{-1}) and ν_{PES} = 2236 cm^{-1} ($\nu_{ab\ initio}$ = 2277 cm^{-1}), respectively.

Results and discussion

Fig. 2 shows the schematic potential energy surface of the $SiH_3Cl + F^-$ system with the classical (adiabatic) energies of its characteristic stationary points.[23] Classical energies are defined as the energies of PES-optimized stationary points referenced to the PES-optimized reactant structure and exclude zero-point vibrational energy, while adiabatic energies are corrected for harmonic zero-point vibrational contributions. The energy values were obtained from our previously-reported potential energy surface.[23] The energetically most favorable reaction is the chloride-ion substitution leading to $SiH_3F + Cl^-$ formation. It is highly exothermic and proceeds through two main mechanisms, the Walden inversion and the front-side attack retention. The Walden inversion follows a single-well potential, passing through the global minimum complex, WMIN. The retention channel is characterized by a double-well potential, featuring two minima, the reactant-like FSPreMIN and the

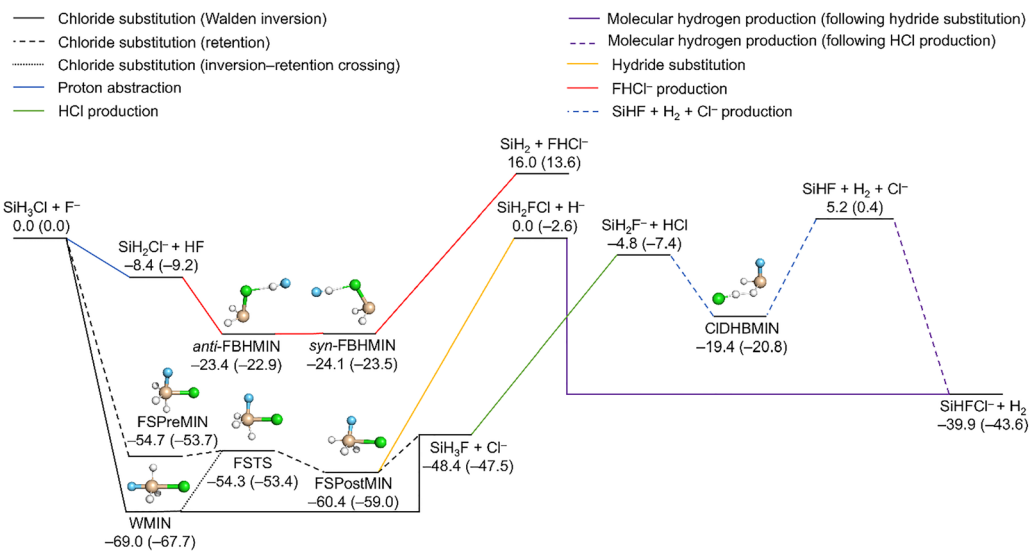

Fig. 2 Schematic potential energy surface of the $SiH_3Cl + F^-$ system featuring the main reaction channels as well as the classical (adiabatic) energies of the minima, transition states and the products relative to the reactants in kcal mol^{-1}.[23,24]

product-like FSPostMIN, connected by the front-side attack transition state, FSTS. These deep negative-energy stationary points ensure that the retention channel remains accessible at low collision energies, competing with inversion.

The stationary points characteristic to the chloride-substitution pathways, namely WMIN, FSPreMIN, FSPostMIN and FSTS can also decay in a near-athermic hydride-ion substitution, resulting in the formation of $SiH_2FCl + H^-$. The proton-abstraction reaction, producing $SiH_2Cl^- + HF$, is a barrierless reaction. Due to its exothermicity and simple mechanism, it is among the most characteristic reactions of the $SiH_3Cl + F^-$ system. The leaving ions of the hydride- and chloride-ion substitutions can perform proton abstractions as well, leading to $SiHFCl^- + H_2$ and $SiH_2F^- + HCl$ formations, respectively. There is also an alternative, multi-step mechanism for molecular-hydrogen production following the chloride substitution and the subsequent $SiH_2F^- + HCl$ production. This process includes the formation of a dihydrogen-bonded complex, ClDHBMIN, which decomposes into three fragments, $SiHF + H_2 + Cl^-$. The recombination of the SiHF and Cl^- fragments is a significant $SiHFCl^- + H_2$ producing pathway at low collision energies. The proton-abstraction reaction can also be followed by halide abstraction through the bihalide ion formation complex FBHMIN (possessing *anti*- and *syn*-conformations), leading to $SiH_2 + FHCl^-$.

Fig. 3 and 4 illustrate the integral cross sections (ICSs, denoted by σ) and cross section ratios ($\sigma/\sigma_{\text{Ground state}}$) as a function of collision energy for the $F^- + SiH_3Cl$ (ν_k = 0, 1) reactions (where k labels the normal modes shown in Fig. 1 and the notation means zero quantum on all the modes other than k), including chloride-ion substitution, proton abstraction, hydrogen-chloride formation, molecular-hydrogen production, hydride-ion substitution, and bihalide-ion formation. The chloride-ion substitution channel is further divided into inversion and retention contributions. To estimate the statistical uncertainty of the cross section ratios, we present Fig. 4 in the

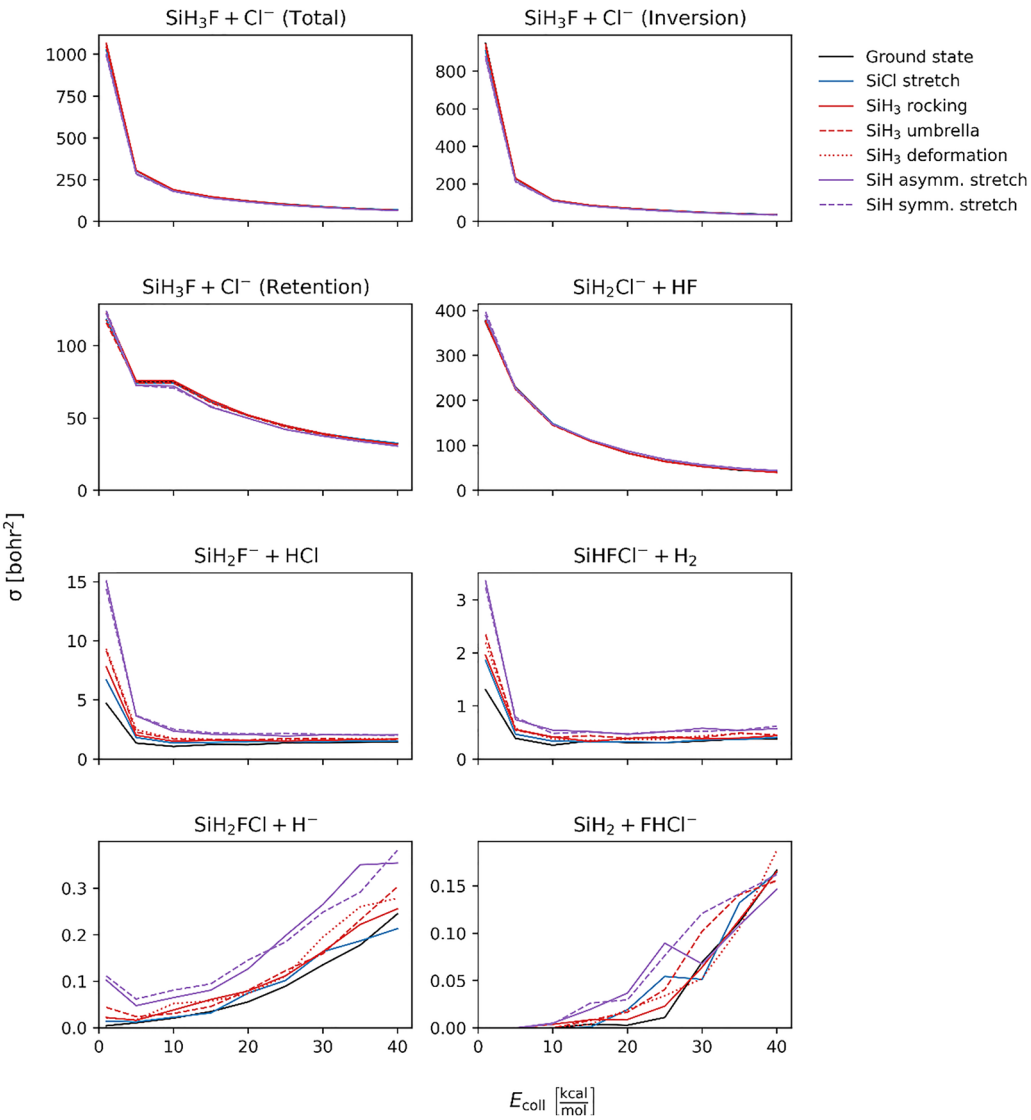

Fig. 3 Mode-specific integral cross sections of the $F^- + SiH_3Cl$ (ν_k = 0, 1) reactions between E_{coll} = 1 and 40 kcal mol^{-1}.

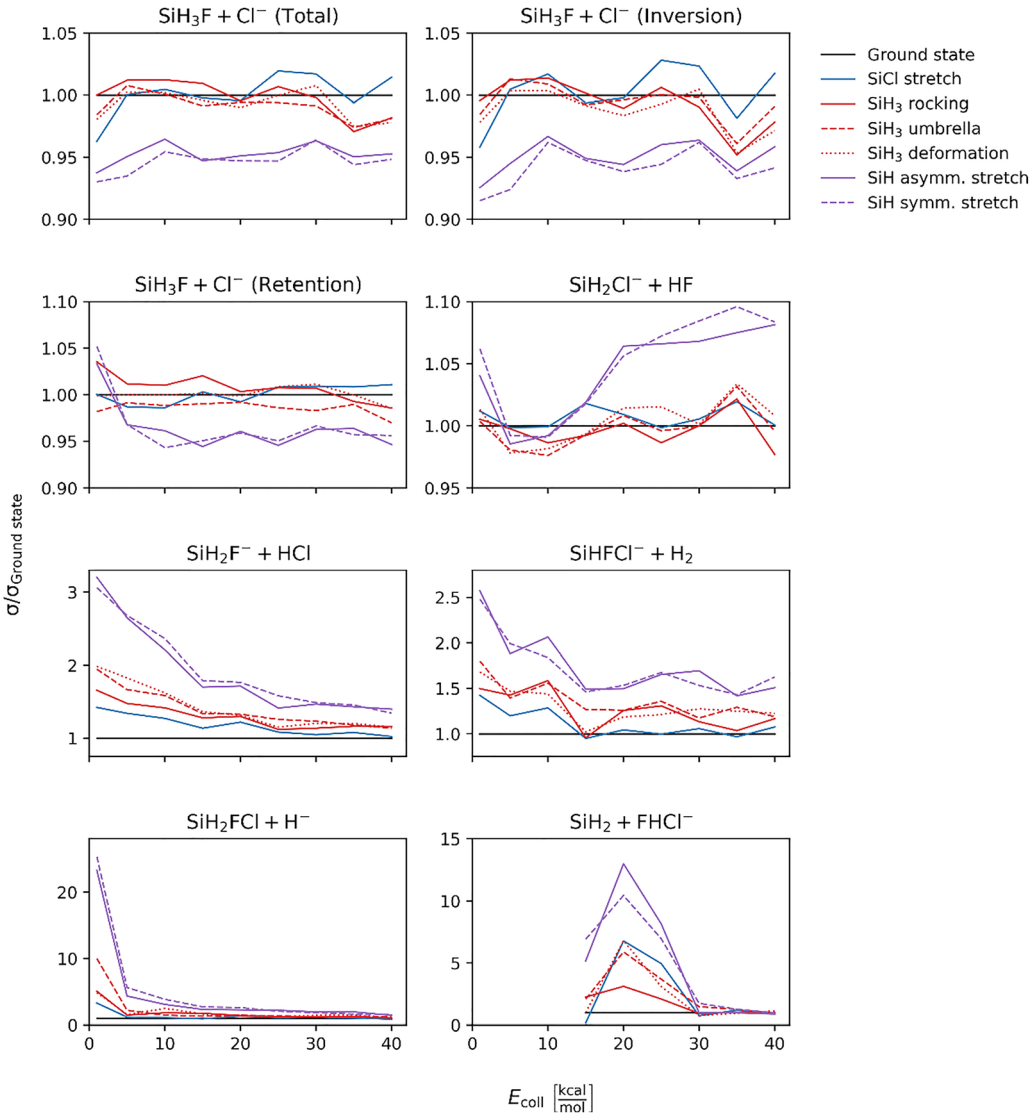

Fig. 4 Mode-specific integral cross section ratios ($\sigma/\sigma_{\text{Ground state}}$) of the F^- + SiH_3Cl (ν_k = 0, 1) reactions as a function of collision energy.

SI obtained by analyzing the first (Fig. S1) and second (Fig. S2) half of the trajectories. As Fig. S1, S2 and Fig. 4 show most of the data are statistically accurate and the features shown in Fig. 4 are well reproduced by the half of the trajectories. The interested reader may compare the results presented in Fig. 4 and discussed below to the data shown in Fig. S1 and S2 to judge their statistical significance.

For collision energies of 1–40 kcal mol^{-1}, the ICS for chloride-ion substitution decreases from approximately 1000 bohr^2 to ~70 bohr^2 in both ground-state and vibrationally-excited simulations. Mode-specific effects are more prominent when comparing the $\sigma/\sigma_{\text{Ground state}}$ ratios instead of the total cross sections, and the minor differences in the preferences for mode-specific excitation in the inversion and retention channels also become apparent. Excitation of the symmetric and asymmetric SiH stretching modes reduces the probability of inversion substitution by approximately 5% across the entire energy range. For the retention channel, this holds true above E_{coll} = 5 kcal mol^{-1}, while at E_{coll} = 1 kcal mol^{-1}, the SiH stretching excitation increases the cross section by 3–5%. The excitation of other vibrational modes has an even milder, almost negligible effect.

The slight inhibition of chloride substitution is likely caused by changes in the entrance channel dynamics. Excitation of the SiH stretching modes may slightly reduce the lifetime or formation probability of the substitution complexes, leading to a modest decrease in the S_N2 cross sections.

In the case of proton abstraction, excitation of the SiH stretching modes increases the ICS by about 5% at the lowest collision energy, while between E_{coll} = 20–40 kcal mol^{-1}, the increase is in the range of 5–10%. Interestingly, in the medium collision energy range, between E_{coll} = 5–15 kcal mol^{-1}, the effect of excitation of SiH stretching modes is negligible. Excitation of the other modes has no impact on the cross section of proton abstraction.

Excitation of every vibrational mode of the reactant molecule substantially enhances the SiH_2F^- + HCl formation pathway

across the entire collision energy range. In the case of the ground-state simulations, the ICSs were 4.7 bohr^2 at a collision energy of 1 kcal mol^{-1}, 1.5 bohr^2 at 40 kcal mol^{-1}, and the smallest cross section of 1.1 bohr^2 was observed at E_{coll} = 10 kcal mol^{-1}. The SiH stretching mode excitations provide the most significant effect, with $\sigma/\sigma_{Ground\ state}$ slightly exceeding 3 at E_{coll} = 1 kcal mol^{-1} and approximately 1.5 at 40 kcal mol^{-1}. Excitation of the SiH_3 umbrella and deformation modes produces $\sigma/\sigma_{Ground\ state}$ ratios ranging from 2.0 to 1.1 as collision energy increases. Excitation of the SiH_3 rocking and SiCl stretching modes yields $\sigma/\sigma_{Ground\ state}$ values of approximately 1.7 at the lowest collision energy and 1.2 at the highest, corresponding to increases of about 70% and 20%, respectively, relative to the ground state.

For molecular-hydrogen production, the collision energy dependence of the ground-state ICS and the influence of reactant vibrational excitation on the cross sections closely resemble those observed in the HCl formation channel. The ground-state ICS peaks at 1.3 bohr^2 at the lowest collision energy, drops to a minimum of 0.27 bohr^2 at E_{coll} = 10 kcal mol^{-1}, and slightly rises to 0.38 bohr^2 at the highest collision energy. For SiH symmetric and asymmetric stretching excitations, $\sigma/\sigma_{Ground\ state}$ reaches 2.5 at E_{coll} = 1 kcal mol^{-1}. Excitation of bending modes and SiCl stretching enhances the ICS by 40–80% at the smallest collision energy. Above E_{coll} = 15 kcal mol^{-1}, the impact of SiCl stretching excitation becomes negligible compared to other modes. At the highest collision energy, the $\sigma/\sigma_{Ground\ state}$ ratio for SiH stretching excitation decreases to 1.5, while ratios for SiH_3 deformation, umbrella, and rocking bending modes are approximately 1.2.

The ICS for hydride-ion substitution increases with increasing collision energy for both ground-state and vibrationally-excited reactants. At the lowest collision energy, E_{coll} = 1 kcal mol^{-1}, the ground-state cross section is nearly zero, making $\sigma/\sigma_{Ground\ state}$ ratios unreliable at low E_{coll} range. At E_{coll} = 40 kcal mol^{-1}, the ground-state cross section for $SiH_2FCl + H^-$ reaches 0.25 bohr^2. Excitation of the SiH stretching modes have the most significant effect on the cross section, with $\sigma/\sigma_{Ground\ state}$ ratios ranging from 3.0 to 3.8 at E_{coll} = 10 kcal mol^{-1} and stabilizing around 1.5 at E_{coll} = 40 kcal mol^{-1}. The ICS-enhancing effect of SiCl excitation is negligible. Excitation of bending modes increases the ICS by approximately 0.02–0.05 bohr^2 across the entire collision energy range.

Vibrational excitation of the SiH stretching modes enhances the Si–H bond cleavage, thereby promoting reaction pathways that feature proton transfer. Most notably, this effect facilitates proton abstraction leading to HF formation, as well as multi-step mechanisms such as H_2 and HCl formation, which involve abstraction event. Since the Si–H bond dissociates in the hydride ion substitution pathway, selective excitation of SiH stretching favors this product channel as well.

For the formation of H_2, HCl, and H^-, the integral cross sections generally increased at lower collision energies for all vibrational excitations and the effect is more significant when exciting higher frequency modes. SiH stretching produced the strongest cross section increase, followed by bending modes, and finally SiCl stretching. In the case of HCl formation, the proton abstraction by the leaving ion following the chloride substitution step is an endothermic process, while the hydride ion substitution reaction is nearly athermic, therefore, additional vibrational energy increases the reactivity of these channels. H_2 formation is linked to both hydride-ion substitution and HCl production, as its characteristic mechanisms involve these processes as intermediate steps. This mechanistic link explains why the excitation of any vibrational mode leads to an overall increase in the H_2 formation cross section.

For the bihalide-formation channel, the cross section is negligible below E_{coll} = 10 kcal mol^{-1} and does not exceed 0.01 bohr^2 below E_{coll} = 25 kcal mol^{-1}. At higher collision energies, the ICS increases rapidly, reaching 0.17 bohr^2 at the highest collision energy. The $\sigma/\sigma_{Ground\ state}$ ratios exhibit maximum values near E_{coll} = 20 kcal mol^{-1} for all vibrational mode excitations. The highest $\sigma/\sigma_{Ground\ state}$ ratio is observed for SiH stretching excitations at E_{coll} = 20 kcal mol^{-1}, reaching 10–13. For other modes, the $\sigma/\sigma_{Ground\ state}$ ratios at E_{coll} = 20 kcal mol^{-1} range from 3.1 to 6.8. At E_{coll} = 40 kcal mol^{-1}, the $\sigma/\sigma_{Ground\ state}$ ratios decrease to approximately 1 for all mode-specific excitations.

The bihalide ion is prone to decomposition resulting in $SiH_2 + HF + Cl^-$, which explains why vibrational excitation produces a smaller $\sigma/\sigma_{Ground\ state}$ enhancement at higher collision energies. In this $FHCl^-$ channel, SiCl stretching excitation has a more pronounced effect on the ICS than the bending modes, consistent with the fact that bihalide formation proceeds *via* halide-ion abstraction following HF formation. At E_{coll} = 40 kcal mol^{-1} the ground-state ICS of $SiH_2 + HF + Cl^-$ is only 0.07 bohr^2, which becomes about 0.3, 0.4, and 0.6 bohr^2 upon SiCl stretching, bending, and SiH stretching excitations, respectively. However, these predictions may have large uncertainties, because the PES does not describe this three-fragment region accurately as discussed in ref. 23.

To place our results into context, we compare them with the mode-specific vibrational excitation effects reported for the carbon-centered $F^- + CH_3I$ system.[15] For S_N2 inversion in $F^- + CH_3I$, the integral cross sections are extremely high at E_{coll} = 1 kcal mol^{-1}, exceeding 1500 bohr^2, and decrease asymptotically with increasing collision energy, closely resembling the overall energy dependence observed in the Si-centered reaction. However, the mode-specific trends differ qualitatively. Below E_{coll} = 10 kcal mol^{-1}, excitation of essentially all vibrational modes inhibits inversion by up to around 10%, whereas at higher collision energies most of the vibrational mode excitations become mildly enhancing, with CI stretching providing 10–20% enhancement, consistent with direct coupling to the bond being broken. This contrasts with the $F^- + SiH_3Cl$ reaction, where inversion substitution is suppressed in the entire collision energy range by $\sim$5% upon SiH stretching excitation, and excitation of other modes, including the SiCl stretching mode, has an even smaller effect. Much larger differences appear for the remaining reactions. In the $F^- + CH_3I$ system, both S_N2 substitution with retention and proton abstraction show very strong mode specificity upon CH stretching excitation. At low collision energies, this excitation significantly increases the cross sections, yielding $\sigma/\sigma_{Ground\ state}$ values of approximately 5–20 for retention substitution and up to nearly 80 for proton abstraction. As the collision

energy increases, these enhancement factors decrease rapidly to around 1 for retention substitution and around 2 for proton abstraction at E_{coll} = 35 kcal mol^{-1}. In the Si-centered system, by comparison, proton abstraction is only weakly mode selective, typically showing less than 10% enhancement, and large $\sigma/\sigma_{Ground\ state}$ ratios are restricted to multistep minor channels such as H_2 and HCl formation, hydride-ion substitution, and $FHCl^-$ formation.

Fig. 5 shows the mode-specific opacity functions of the chloride-ion substitution as well as those of the proton-abstraction channels at small, medium and high collision energies (1, 20 and 40 kcal mol^{-1}, respectively). The opacity function of the chloride-ion substitution channel is divided into retention and inversion contributions.

In the case of the proton-abstraction reaction, the enhancing effect of the SiH stretching modes is observable in the lower impact parameter range, between 0 and 10 bohr at E_{coll} = 1 kcal mol^{-1}, whereas at the highest collision energy the enhancing effect is more pronounced at the peak of the opacity function, at around

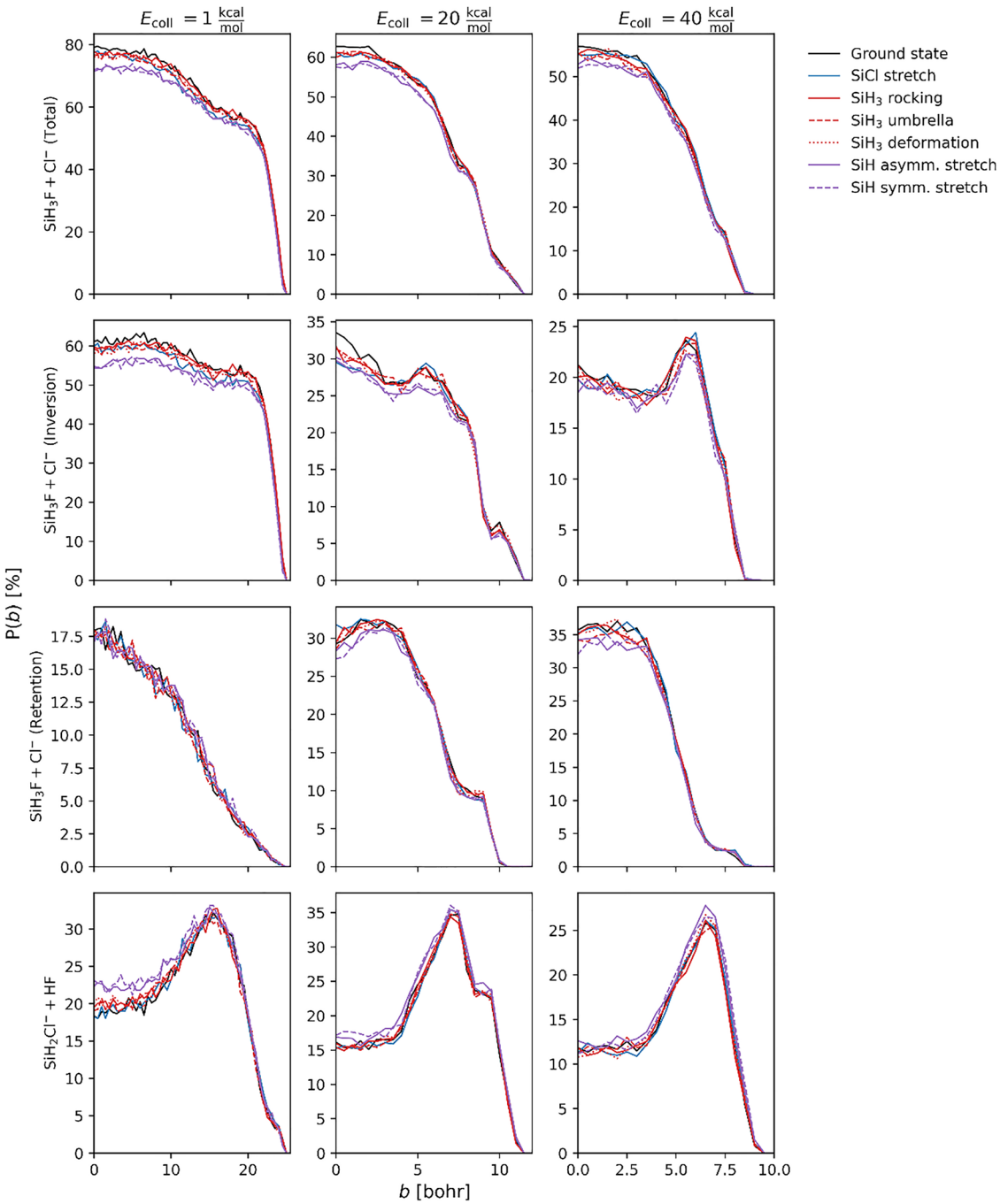

Fig. 5 Mode-specific opacity functions of the F^- + SiH_3Cl (ν_k = 0, 1) chloride-ion substitution (divided into inversion and retention channels) and proton-abstraction reactions at E_{coll} = 1, 20 and 40 kcal mol^{-1}.

b = 7 bohr. At E_{coll} = 20 kcal mol^{-1} the enhancing effect for SiH stretching is significantly less pronounced in the entire impact parameter range. In the discussion of Fig. 4 we noted that the $\sigma/\sigma_{Ground\ state}$ ratios of proton abstraction are increased in the case of SiH stretching excitation for low and high collision energies, but not at medium collision energies. This effect might be the result of different proton-abstraction mechanisms, the direct and the indirect, showing different SiH stretching mode excitation preference patterns.

For the inversion pathway of chloride-ion substitution, SiH stretching excitations lead to a reduction in reaction probability across the entire range of impact parameters and at all collision energies. In contrast, the reaction probability for the retention pathway remains largely unaffected by SiH stretching excitations at the lowest collision energy, though a slight decrease is observed at higher energy. Excitations of other vibrational modes have a negligible impact on the opacity functions for chloride-ion substitution.

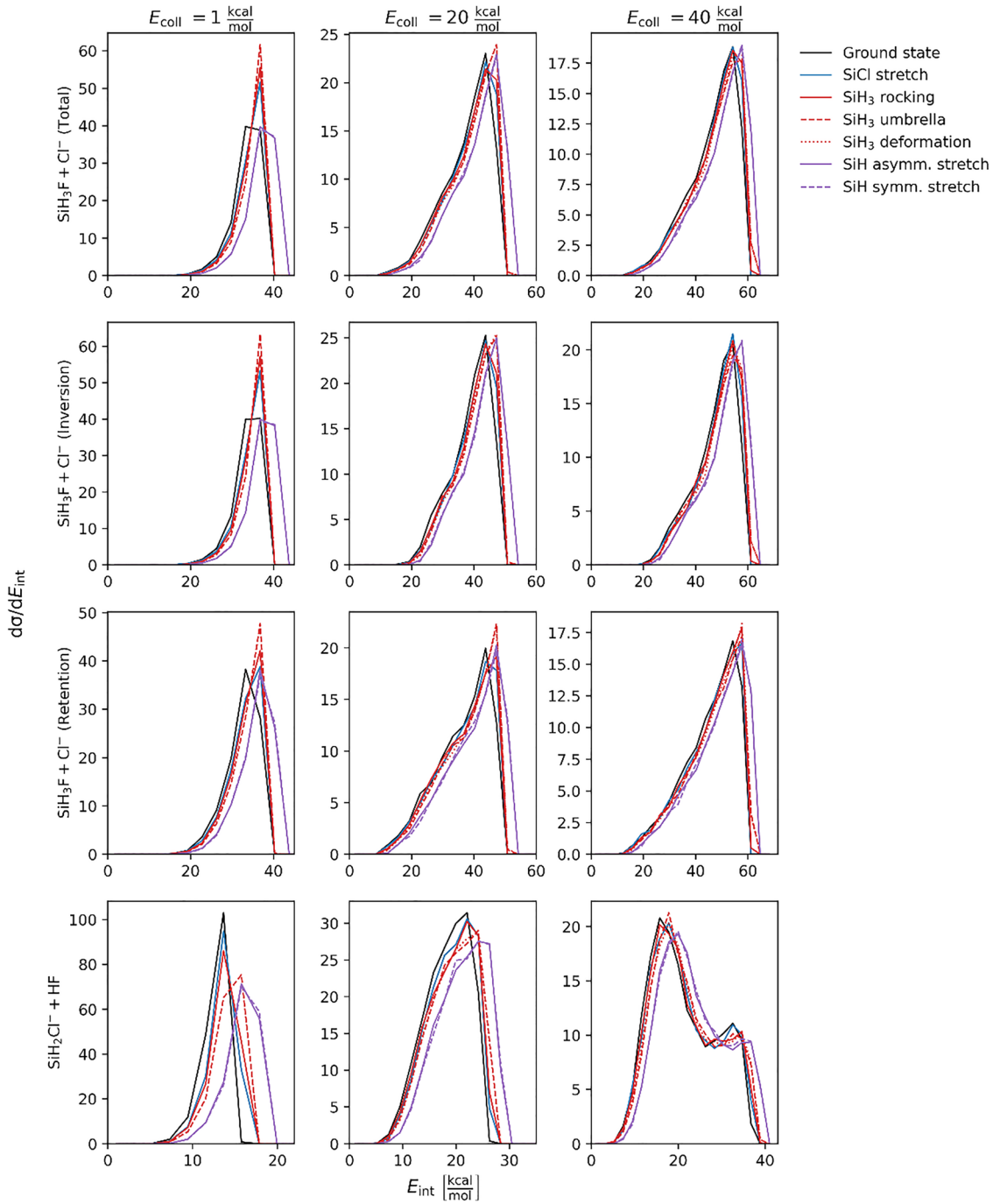

Fig. 6 Mode-specific internal energy distributions of the F$^-$ + SiH$_3$Cl (ν_k = 0, 1) chloride-ion substitution (divided into inversion and retention channels) and proton-abstraction reactions at E_{coll} = 1, 20 and 40 kcal mol^{-1}.

Post-reaction internal energy distributions are depicted in Fig. 6, at E_{coll} = 1, 20 and 40 kcal mol^{-1} in the case of chloride-ion substitution (total, and divided into retention and inversion contributions), and proton abstraction.

Mode-specific excitations have little effect on the internal energy distributions. Distribution profiles remain mostly unaffected, although we can observe consistent shifting to higher energies corresponding to the energy increases of the excitations.

We also investigated the effects of mode-specific excitations for the proton-abstraction and chloride-ion substitution channels on various energy distributions, including translational, rotational, and vibrational energy distributions, as well as on the distributions of the initial attack angle and the scattering angle. Figures illustrating these distributions are provided in the SI.

Rotational energy distributions remain unaffected for either proton abstraction or substitution under any mode excitation. The effects on the vibrational energy distributions correspond to those observed for the internal energy distributions. This is not surprising, as the internal energy can be decomposed into vibrational and rotational components, and the rotational energy distributions did not exhibit any significant changes.

The translational energy distributions for substitution also show only very mild sensitivity to vibrational excitation. At the highest collision energy, for the inversion channel, excitation of the SiH_3 umbrella mode results in a slight decrease in the peak of the distribution, while excitation of the SiCl stretching mode leads to a very slight increase. The translational energy distribution for the retention channel shows no effect.

Mode-specific excitations in the proton-abstraction channel also yield only subtle effects on the translational energy distributions. At the lowest collision energy, excitation of the SiH stretching modes results in a broader translational energy distribution compared to the ground-state case.

Excitation of none of the vibrational modes produced a detectable effect on the initial attack angle or the scattering angle distribution for either proton abstraction or chloride-ion substitution.

Summary and conclusions

Our study investigates the mode-specific quasi-classical trajectory dynamics of the gas-phase F^- + SiH_3Cl reaction on a full-dimensional analytical coupled-cluster-quality potential energy surface. Key reaction pathways explored include chloride ion-substitution (*via* inversion and retention mechanisms) and proton abstraction, alongside secondary reactions such as HCl formation, hydride-ion substitution, molecular-hydrogen production, and bihalide-ion ($FHCl^-$) production. Millions of simulations were run to assess how selective excitation of individual vibrational modes in the reactant SiH_3Cl affects reaction dynamics. Detailed analyzes include opacity functions, cross sections, distributions of initial attack angles and scattering angles, and product energy distributions. Vibrational excitations minimally influenced initial attack and scattering angle distributions. Generally, internal energy distribution of products shifted toward higher energies, proportionally to the vibrational energy input from excitation, while rotational and translational energy distributions were largely unaffected. Exciting the SiH stretching modes slightly decreased chloride-substitution probability and slightly increased the cross section of proton abstraction. Notably, SiH stretching excitations significantly enhanced the cross sections of the low-probability reactions, including HCl and H_2 productions by a factor of 3 and 2.5 at E_{coll} = 1 kcal mol^{-1}, and at E_{coll} = 20 kcal mol^{-1}, $FHCl^-$ production was enhanced by factors of 10 and 13 for symmetric and asymmetric SiH stretching excitations, respectively. Excitations of bending and SiCl stretching modes produced only moderate or negligible effects in chloride-ion substitution and proton abstraction. For the low-probability channels, we observed increased cross sections upon bending and SiCl stretching excitations, similarly, but less significantly, to the effects of the SiH stretching excitations.

Our results demonstrate that the reaction dynamics of silicon-centered systems, such as F^- + SiH_3Cl, can be influenced through mode-specific vibrational excitations. While the dominant pathways, chloride-ion substitution and proton abstraction, show moderate sensitivity to these excitations, the low-probability channels are markedly enhanced, particularly at the lowest collision energies. We hope that these findings will motivate further theoretical chemical studies of silicon-centered reactions, as well as experimental investigations.

Conflicts of interest

There are no conflicts of interest to declare.

Data availability

The data that support the findings of this study are available from the corresponding author upon reasonable request.

Supplementary information (SI): mode-specific cross section ratios obtained from half of the trajectories, as well as initial attack angle, scattering angle, internal energy, translational energy, vibrational energy, and rotational energy distributions for the various channels of the F^- + SiH_3Cl reaction. See DOI: https://doi.org/10.1039/d5cp04412j.

Acknowledgements

We thank the National Research, Development and Innovation Office—NKFIH, K-146759; project no. TKP2021-NVA-19, provided by the Ministry of Culture and Innovation of Hungary from the National Research, Development and Innovation Fund, financed under the TKP2021-NVA funding scheme; and the Momentum (Lendület) Program of the Hungarian Academy of Sciences for financial support.

References

1 G. C. Schatz, M. C. Colton and J. L. Grant, *J. Phys. Chem.*, 1984, **88**, 2971.
2 W. R. Simpson, T. P. Rakitzis, S. A. Kandel, T. Lev-On and R. N. Zare, *J. Phys. Chem.*, 1996, **100**, 7938.
3 S. Yoon, S. Henton, A. N. Zivkovic and F. F. Crim, *J. Chem. Phys.*, 2002, **116**, 10744.
4 J. Sansón, J. C. Corchado, C. Rangel and J. Espinosa-García, *J. Phys. Chem. A*, 2006, **110**, 9568.
5 S. Yan, Y.-T. Wu, B. Zhang, X.-F. Yue and K. Liu, *Science*, 2007, **316**, 1723.
6 G. Czakó and J. M. Bowman, *Science*, 2011, **334**, 343.
7 S. A. Kandel, T. P. Rakitzis, T. Lev-On and R. N. Zare, *Chem. Phys. Lett.*, 1997, **265**, 121.
8 J. Espinosa-Garcia, J. Calle-Cancho and J. C. Corchado, *Theor. Chem. Acc.*, 2019, **138**, 116.
9 D. Papp, J. Li, H. Guo and G. Czakó, *J. Chem. Phys.*, 2021, **155**, 114303.
10 D. Lu and J. Li, *Theor. Chem. Acc.*, 2020, **139**, 157.
11 C. Hennig and S. Schmatz, *J. Chem. Phys.*, 2004, **121**, 220.
12 Y. Wang, H. Song, I. Szabó, G. Czakó, H. Guo and M. Yang, *J. Phys. Chem. Lett.*, 2016, **7**, 3322.
13 Y. Li, Y. Wang and D. Wang, *J. Phys. Chem. A*, 2017, **121**, 2773.
14 M. Stei, E. Carrascosa, A. Dörfler, J. Meyer, B. Olasz, G. Czakó, A. Li, H. Guo and R. Wester, *Sci. Adv.*, 2018, **4**, eaas9544.
15 B. Olasz and G. Czakó, *J. Phys. Chem. A*, 2018, **122**, 8143.
16 T. Michaelsen, B. Bastian, P. Strübin, J. Meyer and R. Wester, *Phys. Chem. Chem. Phys.*, 2020, **22**, 12382.
17 T. Michaelsen, B. Bastian, A. Ayasli, P. Strübin, J. Meyer and R. Wester, *J. Phys. Chem. Lett.*, 2020, **11**, 4331.
18 V. Tajti and G. Czakó, *Phys. Chem. Chem. Phys.*, 2022, **24**, 8166.
19 S. Rao and D. Wang, *Chin. J. Chem. Phys.*, 2023, **36**, 169.
20 J. Qin and J. Li, *Comput. Theor. Chem.*, 2024, **1235**, 114555.
21 D. A. Tasi and G. Czakó, *J. Chem. Phys.*, 2024, **160**, 044305.
22 Y. Wang, Z. Tu, G. Czakó, H. Song and M. Yang, *J. Phys. Chem. A*, 2025, **129**, 6344.
23 A. Á. Dékány and G. Czakó, *J. Chem. Phys.*, 2023, **158**, 224303.
24 A. Á. Dékány and G. Czakó, *Phys. Chem. Chem. Phys.*, 2024, **26**, 10008.
25 B. J. Braams and J. M. Bowman, *Int. Rev. Phys. Chem.*, 2009, **28**, 577.
26 T. Győri and G. Czakó, *J. Chem. Theory Comput.*, 2020, **16**, 51.
27 H.-J. Werner, P. J. Knowles, G. Knizia, F. R. Manby, M. Schütz, *et al.*, *Molpro, version 2015.1, a package of ab initio programs*, see https://www.molpro.net.
28 W. L. Hase, *Encyclopedia of Computational Chemistry*, Wiley, New York, 1998, pp. 399–407.
29 L. Verlet, *Phys. Rev.*, 1967, **159**, 98.
30 See https://gitlab.com/d_attila/qcta for the source code of the qcta (quasi-classical trajectory analyzer) Python package.
31 See https://d_attila.gitlab.io/qcta/index.html for the online documentation of qcta.
32 T. B. Adler, G. Knizia and H. J. Werner, *J. Chem. Phys.*, 2007, **127**, 221106.
33 T. H. Dunning, Jr., *J. Chem. Phys.*, 1989, **90**, 1007.